REVIEW ARTICLE

Check for updates

Plasmon-induced hot-hole generation and extraction at nano-heterointerfaces for photocatalysis

Monika Ahlawat [1], Diksha Mittal[2] & Vishal Govind Rao [1]✉

Localized surface plasmon resonance excitation presents tremendous opportunities for light-harvesting in the field of photocatalysis. Notably, the use of plasmon-generated hot carriers to drive chemical reactions offers the opportunity to control the selectivity of the reaction, unlike temperature-driven catalysis. There has been extensive development of photocatalysts based on plasmon-induced hot electron transfer. However, the equally important hole transfer process has been largely understudied mainly because of the ultrafast dynamics and shorter lifetime of holes compared to electrons. The electron and hole transport asymmetry to the catalytic site introduces additional challenges in extracting holes as oxidants for chemical adsorbents/reactants. This review provides a fundamental overview of plasmonic catalysis, emphasizing recent hot hole extraction and catalysis advancements by exploring different nano-heterointerfaces through which energetic holes can be localized to the catalytic sites. We also highlight some of the critical parameters which must be considered to address the limitations and introduce new possibilities to the field.

Plasmonic metal nanostructures interact strongly with incident electromagnetic radiation by activating localized surface plasmon resonance (LSPR). The realization that the LSPR excitation allows subdiffraction-limit field localization and unusually high field enhancement enables tremendous opportunities for light-harvesting in the field of photocatalysis[1]. The high field energy near the nanoparticle surface gets dissipated through either the radiative scattering of a photon or via the non-radiative decay, generating non-equilibrium distribution of hot charge carriers. Depending upon the nanomaterial's electronic band structure, the charge carrier's potential energy determines their contribution to the total free energy of chemical reactions occurring on the nanoparticle surface[2,3]. Thus, these hot charge carriers hold great promises in altering the potential landscape of thermodynamically as well as kinetically challenging chemical reactions. However, the ultrashort lifetime and the short mean free paths are still some of the fundamental barriers to overcome for the efficient extraction and utilization of these hot charge carriers[4].

Charge carrier-driven chemical reactions on bulk single-crystalline metal surfaces were carried out in the 1990s, providing experimental evidence for improved product selectivity using high-intensity short-pulse lasers[5,6]. However, the use of high-intensity laser sources seems impertinent to industrial applications. Since the plasmon-generated hot electron–hole pairs were realized, various theoretical and experimental model systems, including hybrid heterostructures, have been designed to understand and execute the efficient extraction of plasmon-induced electrons via direct or indirect pathways. Hot electrons have been utilized as a reductant in numerous chemical reactions[7,8]. On the contrary, hot holes were either compromised with hole scavengers or underwent a concomitant reaction sequence with solvents present in the reaction mixture.

[1] Department of Chemistry, Indian Institute of Technology Kanpur, Kanpur 208016 Uttar Pradesh, India. [2] Department of Chemical Sciences, Indian Institute of Science Education and Research, Berhampur 760010 Odisha, India. ✉email: vgrao@iitk.ac.in

This can be because of the asymmetric distribution of hot electrons and holes and the shorter lifetime of holes (because of low group velocities and short mean free path of holes) compared to the electrons in noble metals[3,9]. In particular, the high-energy holes generated in the d-band of noble metals possess large effective mass and low kinetic energy. Hence holes generated within nanoparticles undergo thermalization without reaching the surface[10]. This asymmetry in the electron and hole transport to the catalytic site introduces additional challenges in the extraction of holes as an oxidant for chemical adsorbents/reactants.

Recently, researchers in the field have diverted their attention towards extracting hot holes by exploring different interfaces through which energetic holes can be localized to the catalytic surface to achieve efficient charge separation. The metal–semiconductor interface is one of the promising interfaces being explored to extract hot holes for driving reactions such as oxygen evolution reaction, oxidative polymerization of organic monomers, and oxidation of various organic molecules[11–14].

In this review, we will first understand the mechanism underlying plasmon decay dynamics and the processes involved in generating energetic charge carriers with particular attention to holes. We will highlight different strategies/mechanisms adopted to extract hot holes from the plasmonic metals. Further, we will review the advancements in plasmonic catalysis, highlighting hot holes driven chemical reactions and their impact on the ongoing catalysis research. Finally, we will list out some of the critical parameters which need to be revisited to minimize the fundamental limitations of the field and introduce new possibilities to the area of plasmonic catalysis.

Plasmon excitation and characteristics of absorption processes in plasmonic metals. Plasmonic metal nanoparticles are light-harvesting materials, which interact strongly with incident electromagnetic radiation by activating LSPR. Upon light irradiation with a wavelength greater than the size of the nanoscale particle, the feature of LSPR induces strong oscillation of the free electrons of metals in phase with the incident light's electric field (Fig. 1a). The resonance condition is achieved when the photon frequency matches with the frequency of the free electrons oscillating against the restoring force of the nuclei. As a consequence of plasmon excitation, the irradiated light energy gets confined as elevated local electric fields near the surface of the metal nanoparticles. The distribution of these confined electric fields remains spatially inhomogeneous, being maximum at the surface[15,16]. In the intense near field regions known as plasmonic hotspots (created between two closely spaced nanoparticles), the field intensity can be enhanced by a factor of 10^4–10^6[17]. These elevated LSPR fields stimulate a cascade of events on a timescale of femto-seconds (fs) to nanoseconds (ns) and dissipate the energy via radiative or non-radiative decay, where the latter leads to the generation of electron–hole pairs (Fig. 1b)[15]. The absorption and subsequent generation of electron-hole pairs can occur via four following pathways (Fig. 1c–e). Firstly, consider the electronic band structure of a metal having two states with wavevectors, i.e., momenta $\mathbf{k_1}$ and $\mathbf{k_2}$, and energies below and above the Fermi level (E_F) as E_1 and E_2 with $E_2 = E_1 + \hbar\omega$, respectively. The absorption process requires an imperfection or a phonon so that the momentum remains conserved, and that eventually leads to the generation of a hot electron and hole via intraband excitation from a filled s state below the Fermi level to an empty s state above (Fig. 1c, blue arrows), where the average energy of each carrier is $\hbar\omega/2$. Nanoparticles with a diameter within tens of nanometers exhibit a rate constant of 10^{13}–$10^{14}\,s^{-1}$ for this type of excitation[9,18]. Secondly, absorption can occur by direct 'diagonal' process known as Landau damping, where the momentum is conserved by the collision of electrons with the surface (Fig. 1c, red arrow). In this process, the surface plasmon polariton mode includes spatial frequencies larger than the difference between the wavevectors of the two states ($\mathbf{\Delta k}$). This intraband transition leads to the formation of hot electron and hole in the s-band with an average energy of $\hbar\omega/2$, and the rate of excitation is affected mainly by the size of the nanoparticle as $\gamma \sim v_F/R$, v_F being the Fermi velocity and R being the radius of the nanoparticle[15,19]. Thirdly, intraband absorption can occur through electron–electron scattering where the momentum is
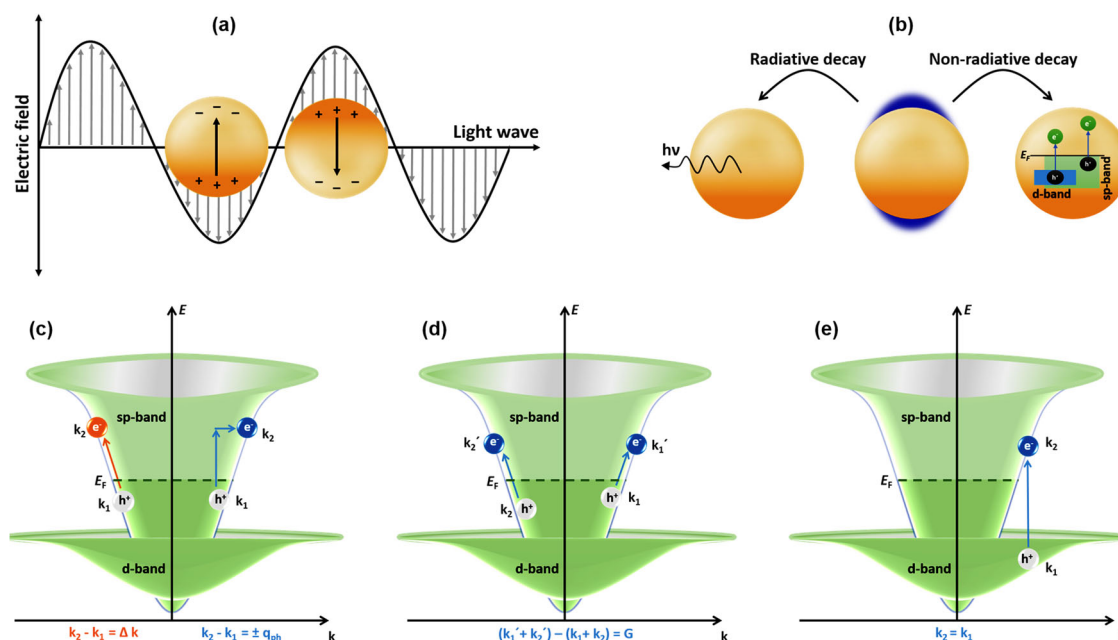

Fig. 1 Plasmon excitation and decay through electronic excitation. a Interaction of electromagnetic radiation with plasmonic metal nanoparticle and LSPR excitation. **b** The dissipation of high local electric fields near the surface of the metal nanoparticles via radiative or non-radiative decay. **c** Indirect, intraband s-to-s, phonon-assisted (blue arrow) and surface collision-assisted "diagonal" transitions (orange arrow). **d** Indirect, intraband s-to-s, electron–electron scattering-assisted transition where the momentum is conserved via the Umklapp process. **e** Direct, interband d-to-s transition (adapted from ref.[10]).
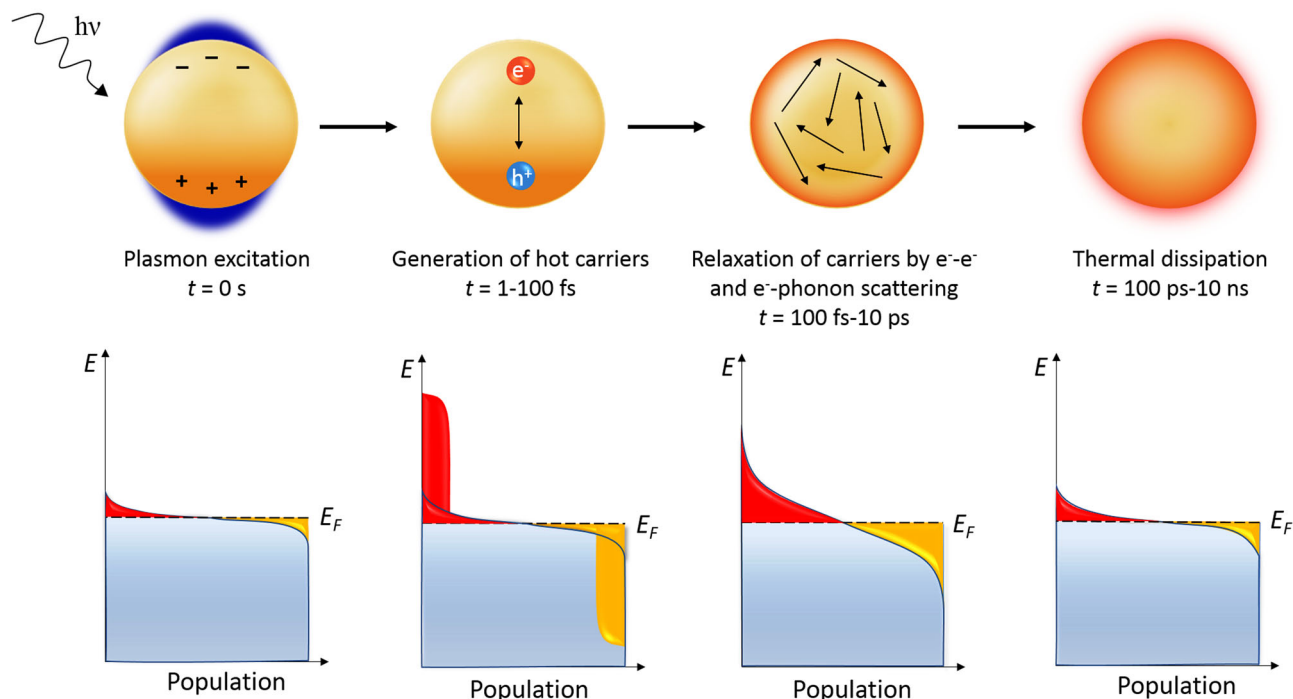
Fig. 2 Dynamics of plasmon decay and time evolution of charge carriers. Plasmon excitation at $t = 0$ and subsequent generation of athermal (not describable using Fermi-Dirac statistics) hot electron–hole pairs within the metal, then thermalization via electron–electron, electron–phonon scattering (this leads to a Fermi-Dirac distribution of charge carriers representing elevated temperature) and further via thermal dissipation via phonon–phonon scattering. E_F indicates Fermi level, and yellow and red areas indicate holes and electrons energy, respectively. (Adapted with permission from ref. [24] Copyright © 2016, American Chemical Society).

conserved in the Umklapp process, that is, the addition of a reciprocal lattice vector to the result of the addition of two initial wavevectors (Fig. 1d). It leads to the formation of four 'lukewarm' carriers from a single photon rather than just two that share the energy $\hbar\omega$, such that the average energy of each carrier becomes $\hbar\omega/4$. This process occurs with a rate constant of $\sim 10^{15} (E_{ph}/E_F)^2 \, s^{-1}$, E_{ph} being the photon energy[15,19,20]. Fourthly, there can be d-band to s-band interband excitation, where the momentum remains conserved (Fig. 1e), and this results in a relatively higher characteristic rate constant of $\sim 10^{15} \, s^{-1}$ [18]. The electrons generated from this excitation are not very energetic as they are generated close to the Fermi level. In contrast, highly energetic holes are generated in the d-band, although their extraction is a challenge discussed in the following sections.

To simplify all four processes, we can say that the generation of charge carriers by non-radiative decay can be through intraband s-to-s excitation or interband d-to-s excitation where direct interband with a high rate constant excitations tend to be a dominant decay pathway when energetically accessible[3]. Noble metals, especially Ag, have their d-bands located far below the Fermi level, and hence interband excitations cannot be induced by visible light. However, Au and Cu have d-bands located closer to the Fermi level than Ag; hence, interband transitions can be induced by visible light above a specific threshold. Contrastingly, in non-noble metals, the d-states are not full and intersect the Fermi level to exhibit interband transition in the entire visible range.

Dynamics of plasmon decay. After plasmon excitation and charge carrier generation within a short time of 1–100 fs, the charge carriers further undergo the steps of electron–electron relaxation, electron–phonon relaxation, and phonon–phonon relaxation (Fig. 2)[21,22]. Primarily, a hot electron–hole pair generated from plasmon decay dissipates its energy via electron–electron scattering on a 100 fs–1 ps timescale. A hot

electron above the Fermi level collides below, quickly redistributing its energy to many lower-energy electrons. Another relaxation pathway includes electron–phonon scattering on a 1–10 ps timescale where the electrons collide with the metal's ionic lattice causing heating of the nanoparticle, as well as phonon–phonon scattering spawning vibrations in the metal lattice on a 100 ps–10 ns timescale, that results in heating up of the local surroundings, thus loss of energy to the environment[23,24].

Hot electron vs. hot hole: energetics, lifetime and transport. The energy distribution of hot charge carriers generated in plasmonic metals has been of great interest since ever to manipulate the various applications in photocatalysis. The electronic band structure of the plasmonic metals determines the energy distribution of hot charge carriers, for which various theoretical and experimental elucidations have been made[25]. In the case of s-to-s indirect intraband excitations (dominant in Ag at LSPR frequency), there is a generation of hot electrons and holes of relatively equal energies in the s-band of the metal due to the symmetric nature of the s-band around the Fermi level. Whereas considering d-to-s direct interband excitations, Au and Cu exhibit generation of low-energy electrons in the s-band and hot holes in the d-band (Fig. 3a)[3]. The relative position of the s and d-band of the plasmonic metal can modulate the energy distribution of the hot charge carriers, and the electron–phonon interactions can control hot carrier energy loss and transport[26].

In addition to the appropriate energy, the hot carriers generated from plasmon excitation need to have enough lifetime and mean free path so that they can be detected, collected, or extracted before thermalization. In this regard, the lifetime and mean free path of the hot carriers generated in the metals can be presented as a function of the energy and electron–electron and electron–phonon scattering events (Fig. 3b, c)[3,26]. When the charge carriers have low energy close to the Fermi level, the electron–phonon scattering dominates. In
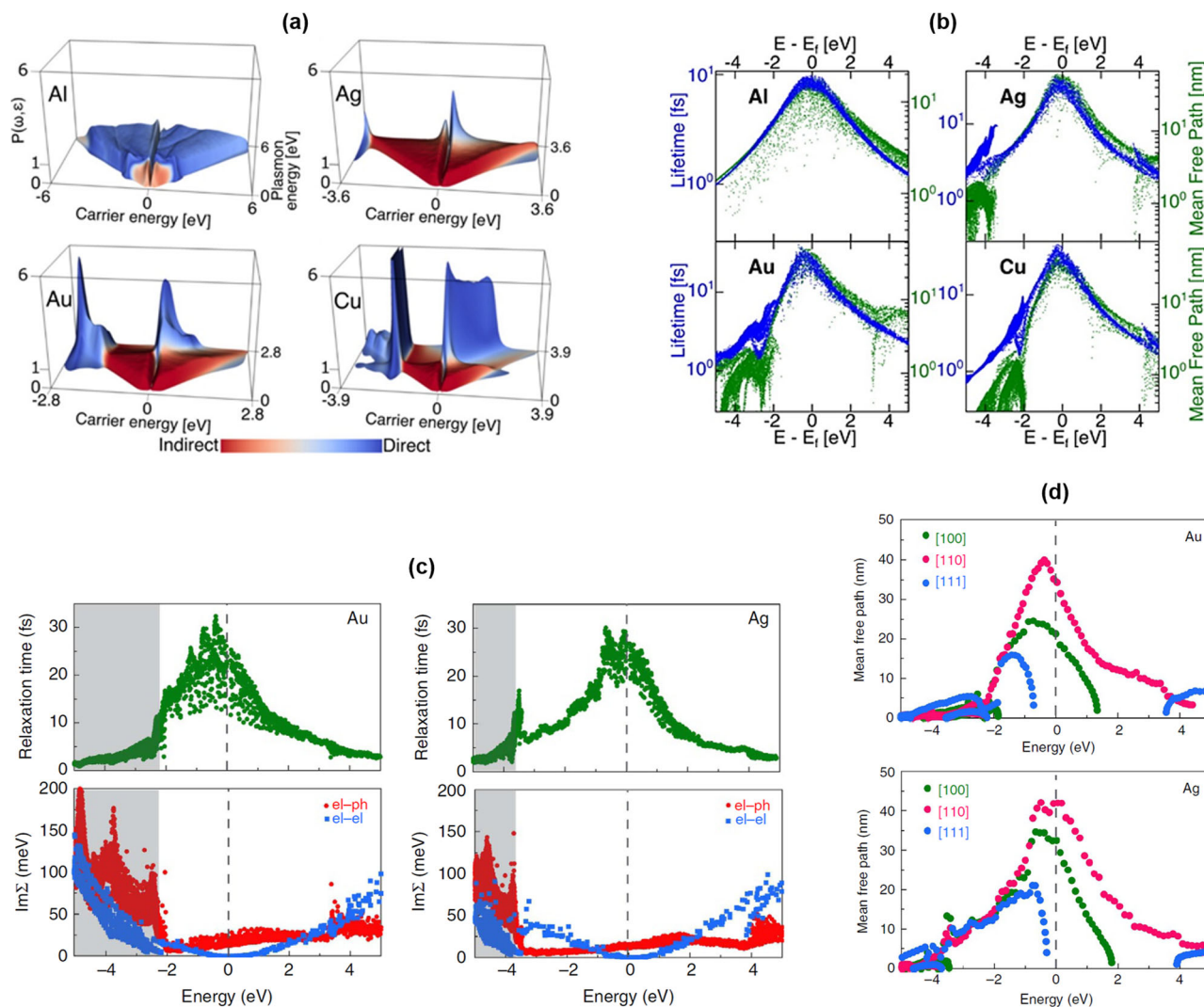
Fig. 3 Energy distribution, lifetime, mean free path, and scattering rates of charge carriers. a The Energy distribution of charge carriers, P(ω,ε) in Al, Ag, Au, and Cu metals as a function of plasmon frequency, ω, and carrier energy, ε. **b** Lifetime and mean free path of charge carriers considering electron–electron and electron–phonon scattering (**a**, **b** reprinted with permission from ref. [3] Copyright © 2016, American Chemical Society). **c** Relaxation time and scattering rates for charge carriers, where scattering rate is expressed as the imaginary part of the self-energy, ImΣ for electron–electron and electron–phonon scattering. The grey shaded area indicates the energy of d-bands. **d** The mean free path of charge carriers along [100], [110], and [111] crystallographic directions, highlighting isotropic mean free path for s-state and anisotropic for d-states (**c**, **d** reprinted from ref. [26]).

contrast, electron–electron scattering remains negligible, resulting in the longest lifetime and mean free path. As such, a maximum lifetime of ~30 fs and a mean free path of ~50 nm can be obtained in the order of Ag > Cu > Au. In contrast, as the energy of the charge carriers increases away from the Fermi level, the electron–electron scattering increases that significantly reduces the lifetime and mean free path to ~10 nm in Au, Ag, Cu, and Al. Apart from the scattering event, the group velocity of electrons and holes also acts as a parameter for determining their respective mean free paths. At similar energies and thus lifetime, the electron having higher group velocity exhibit a higher mean free path. In contrast, d-band holes show a much smaller mean free path because of their smaller group velocities. So, we can safely say that the energy distribution, relaxation time, and mean free path of the hot charge carriers are dramatically different in two regimes of intraband excitation and interband excitation of plasmonic nanomaterials[26].

Charge carrier transport can be altered across various interfaces and is majorly governed by the energetics of hot electrons and holes[4,27]. While engineering interfaces for hole localization, we encounter multiple shapes of nanoparticles, so it is essential to

account for carrier transport to the geometry of the metal. Louie and coworkers characterized the mean free path for Au and Ag in [100], [110], and [111] crystallographic directions up to 5 eV from the Fermi energy (Fig. 3d)[26]. Hot holes with the energy of 1–2 eV (s-band holes) exhibited nearly isotropic mean free path whereas longer mean free path for [100] and [110] directions were observed for hot holes within < 1 eV. However, a highly anisotropic mean free path was obtained in all directions in the d state (d-band holes) of the order 1–5 nm. This observation corroborates the results of ballistic electron energy microscopy experiments and suggests a mean free path for s state to be isotropic and d state of being anisotropic[28]. Clearly, a significant challenge arises when extracting hot holes due to their ultrashort lifetime, shorter mean free path, and faster relaxation dynamics[29]. Significant efforts are required to dodge this constraint, as discussed in the later sections.

Experimental evidence of energy distribution and charge-transport across interfaces. Most of the theoretical studies mentioned above rely on a given set of assumptions about the

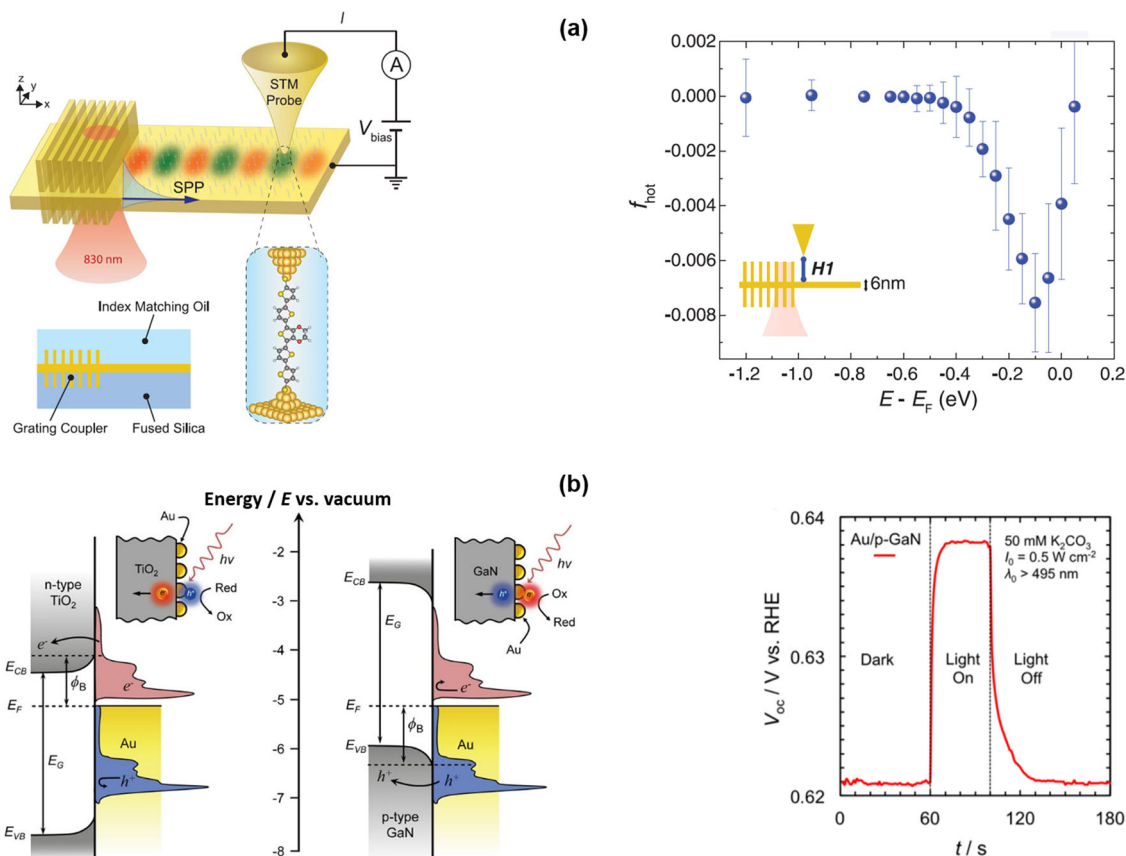**Fig. 4 Demonstration of energy distribution and charge separation across interfaces. a** Schematic of the experimental setup to determine charge-carrier energy distribution by forcing the electrical current through the suitably chosen molecular level and measured hot-hole energy distribution in a 6-nm-thick Au film. (from ref. [33] reprinted with permission from AAAS). **b** Energetically tailored Au/p-GaN interface to localize hot holes to p-GaN (Au/TiO$_2$ system demonstrate that holes cannot cross the interface) and a positive shift in open-circuit voltage (V$_{oc}$) of Au/p-GaN under visible light irradiation (reprinted with permission from ref. [34] copyright © 2018, American Chemical Society).

properties of materials and dominant relaxation pathways that might sometimes cause certain uncertainties. In this regard, experimental investigations have also been made to understand better the distribution of hot charge carriers in plasmonic nanoparticles[30]. The relaxation dynamics and energy distribution of hot carriers have been studied by coupling the metal nanoparticle with non-plasmonic metals or semiconductors, that is, by achieving charge ejection[12,31,32]. Yu et al.[32] used wavelength-dependent scanning electrochemical microscopy to quantify the energy distribution of hot carriers induced at Au/TiO$_2$ nanostructures. Following electron injection from metal into the semiconductor, molecular probes with different redox potential can track the energy distribution of the holes generated at the nano-heterointerface. Moreover, a scanning tunneling microscope with an Au tip was employed to get direct experimental results regarding energy distribution over Au nanofilms of 6- and 13-nm thickness by creating single-molecule junctions between the probe tip and the nanofilms (Fig. 4a)[33]. Transport measurements by forcing the electrical current through the suitably chosen molecular level provide energy distribution of hot electrons and holes.

Careful design of metal–semiconductor interfaces through which energetic holes can be localized to the catalytic surface requires knowledge of metal and semiconductor band structure and band-bending at the interface. Atwater and coworkers fabricated Au/p-GaN and Cu/p-NiO Schottky junctions tailored to study the plasmon-induced hot hole injection across the heterojunction[34,35]. The plasmon-induced holes via interband transitions were hot

enough to be injected over >1 eV Schottky barrier height. They could be successfully collected at the p-GaN valence band (Φ_B = 1.1 eV) (Fig. 4b). The accumulation of hot holes and the charge separation across the Au/p-GaN interface were validated by a positive shift in the open-circuit voltage under visible light irradiation. These results of injection of hot holes that are 1.1 eV below the Fermi level of Au and have high oxidizing power thus acknowledge substantial anticipations in plasmonic photochemistry.

The ultrafast dynamics of non-thermalized hot carriers and particularly the temporal evolution of hot holes in Au/p-GaN, metal–semiconductor heterostructures was also carefully investigated[36]. The 530 nm pump wavelength was employed to generate the hot carriers in Au nanoparticles. Then, to spectrally differentiate, the hot hole dynamics in the p-GaN valence band were probed across the infrared region, and hot electron dynamics in the metal were probed across the visible region. It was considering the dynamics of hot holes, that a sharp rise in the transient absorption (ΔAbs) of Au/p-GaN heterostructure within <200 fs time was observed when probed at 4.85 μm wavelength, in contrast to the negligible ΔAbs obtained for bare p-GaN, which thus confirmed the optical excitation and injection of hot holes in the p-GaN valence band in Au/p-GaN[36]. On the other hand, the injection of hot holes considerably alters the dynamics of hot electrons by increasing the metal's electron density, thereby altering the electronic heat capacity and electron–phonon coupling time. Hence, by knowing the dynamics, the energy distribution can be tailored as well to achieve the desired photocatalytic applications.

Interestingly, a demarcation between the injection and collection of hot holes and electrons was made by studying Cu nanoantennas on p-type GaN and n-type GaN, respectively[37]. Upon interband excitation, a drop in the internal quantum efficiency (IQE) occurred for hot electron collection, whereas a favorable IQE was achieved for hot hole collection. However, with an increase in carrier energy, the relatively much more significant decrease in the mean free path of hot holes than that of hot electrons affected its transport and consequently the device performance[37]. Such experimental comparisons, along with the knowledge of dynamics and energy distribution, can provide guidelines for careful consideration of both the advantages and the disadvantages associated with hot hole collection and thus determine the operational regime in which the device can be optimally functional.

Extraction of hot charge carriers. Extraction of plasmon-induced hot carriers before they thermalize back to the Fermi level is necessary for redox reactions. Given the ultrashort lifetime of the charge carriers (tens of femtoseconds), carrying out multi-carrier reactions having slow kinetics (milliseconds to seconds) is a major challenge[38]. Hence, for timely extraction of the hot charge carriers and extension of their respective lifetimes, various approaches can be made in which coupling of plasmonic metal to a semiconductor has been a promising strategy[19]. In this, the phenomenon of plasmon-induced charge separation (PICS) occurring at the interface of the metal and the semiconductor has widely been used in photovoltaics, photocatalysis, and other applications[39,40]. A conventional mechanism for this remains the plasmon-induced hot electron transfer mechanism involving hot-electron transfer into the semiconductor upon excitation via Landau damping. Another includes direct metal-to-semiconductor interfacial charge-transfer transition involving direct excitation of an electron from metal to the semiconductor[9,41,42]. There has been an avalanche of reports, including highly focused reviews on electron injection in semi-conductors coupled with plasmonic metal nanostructures[43,44]. Recently, Tatsuma and coworkers have reviewed the PICS mechanism and its various applications[43]. However, in this regard, the behavior of hot holes to achieve oxidation reactions via PICS is not well understood. When the semiconductor behaves as an electron transport material (ETM), the oxidation reactions can be performed on the metal nanoparticle either by hole ejection in which hot holes facilitate oxidation via trap sites or by charge accumulation in which hot holes get accumulated in the metal nanoparticle, create a positive shift in the potential, and carry out the oxidation reaction[45].

Incorporating a hole transport material (HTM) (including a p-type semiconductor) to the metal nanoparticle can result in a more effective hot hole injection into the valence band or the highest occupied molecular orbital of HTM. PICS mechanisms can also be studied in such systems[46]. Hot holes possessing sufficient energy to surpass the barrier at the metal–HTM interface may undergo two different injection mechanisms: (i) simultaneous injection of electrons and holes directly into the ETM and HTM, respectively (Fig. 5a), and (ii) stepwise injection of electron of one pair into the ETM and the hole of the other into the HTM, where recombination occurs between the remaining hole and electron of the former and the latter pair (Fig. 5b). The stepwise injection occurs with a higher probability because of the lower energy barrier at the interface. When the
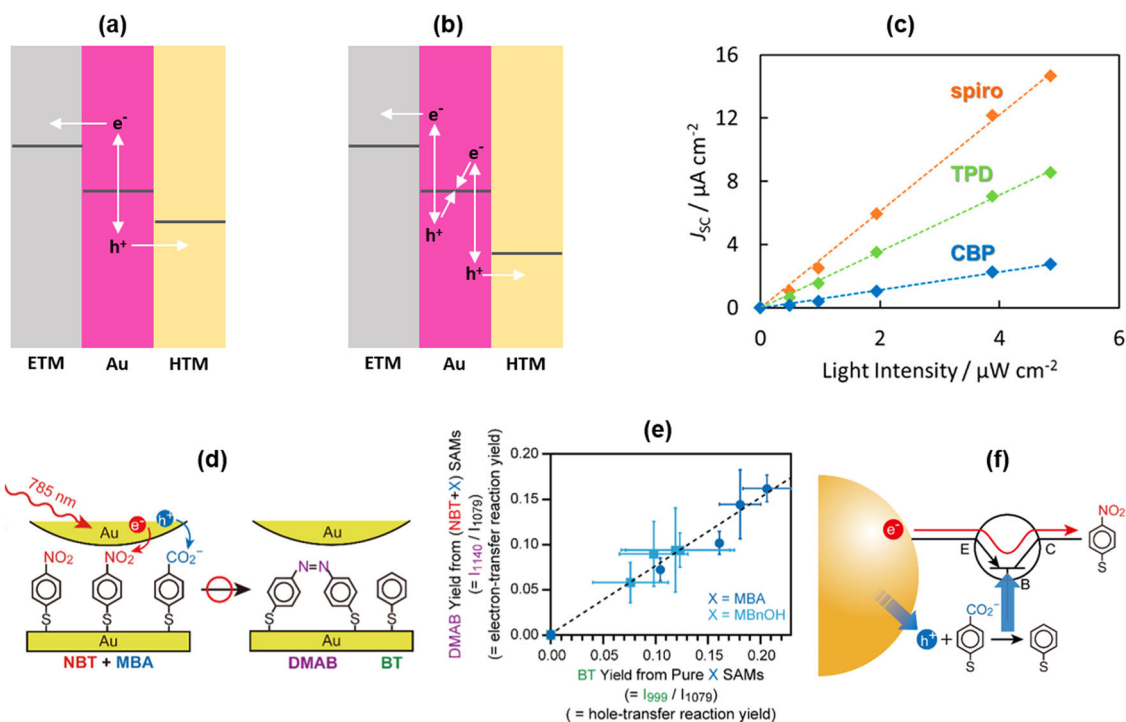

Fig. 5 Strategies for extraction of charge carriers. a Simultaneous and **b** stepwise injection of charge carriers to ETM and HTM. **c** Short-circuit photocurrent, J_{SC} at 600 nm for the ETM–metal–HTM (E–M–H) cells with different HTMs and its dependence on the light intensity, for a fixed intensity, the photocurrent decreases with increasing barrier height for hole transport (**a**, **b** adapted with permission from ref. [46] Copyright © 2019, American Chemical Society and **c** reprinted with permission from ref. [46] Copyright © 2019, American Chemical Society). **d** The hole capture by MBA allows subsequent electron transfer to NBT, resulting in the formation of the DMAB product. **e** A linear relation between electron transfer and hole transfer reaction highlights the importance of hole extraction. **f** Schematic representation of a hole transfer channel, which regulates the flow of electrons by turning the transfer channel on or off. **d**, **f** Reprinted with permission from ref. [51] Copyright © 2020, American Chemical Society.

photocurrent versus light intensity for different HTMs was studied, it was confirmed that the hot electron injection into TiO_2 and hot hole injection into HTM also occurred[46]. The photocurrent decreased with increasing barrier height at the Au–HTM interface, indicating the importance of hole transport (Fig. 5c). Also, when metal–HTM (M–H) cells were studied, maximum external quantum efficiency was obtained for minimum barrier height. The charge separation occurs because of hole injection at the M–H interface, and that the photocurrent is enhanced in the presence of ETM because of better charge separation. Similar studies over ETM–metal–HTM (E–M–H) cells have been conducted by other researchers as well[47,48]. In such systems, efficient hole trapping requires sincere consideration of the energy level for trapping and the thinness and compactness of the HTM. In addition to plasmonic metal nanoparticles, the PICS mechanism has also been studied on plasmonic compound nanoparticles, where hole injection was achieved from MoO_{3-x} nanostructure to the valence band of TiO_2[49] as well as from CuS nanostructure to the CdS valence band[50]. Hence, further such explicit studies on PICS processes, especially hole capture, would enable us to construct devices with better hole extraction to allow oxidation reactions at a higher potential.

Multicomponent designs for hole extraction. Various new design principles have been introduced to thoroughly explore PICS so that the lifetime of the hot carriers can sufficiently be increased and the flow of the plasmonic energy can be biased to the active sites. Such modifications include introducing HTMs and ETMs as already discussed above, hole scavengers, cocatalysts, coupling with semiconductors, metals, and molecules. The importance of hole extraction can be realized in dimerization of 4-nitrobenzenethiol (NBT) to 4,4′-dimercaptoazobenzene (DMAB) over Au nanoparticles by employing mercaptobenzoic acid (MBA) as the hole acceptor (Fig. 5d–f)[51]. NBT requires 4 electrons to reduce to DMAB. Although the energy of hot electrons generated by plasmon excitation in Au is favorable to initiate the reduction of NBT, the reaction cannot proceed without external agents like $NaBH_4$ or HCl[52,53]. The incorporation of MBA with NBT allows hole transfer to MBA, and subsequent electron transfer to NBT results in the formation of DMAB product[51]. The linear correlation obtained in the plot between DMAB surface-enhanced Raman spectroscopy (SERS) peak intensity for electron transfer and hole transfer reaction yield validates the importance of hole extraction. So, the flow of electrons to the collector from the emitter can be controlled by employing a hole transfer channel to regulate the motion of electrons by turning their transfer channel on or off.

It has become common to include hole (or electron) scavengers to enhance reduction (or oxidation) reactions. The importance of hole scavengers can be realized considering the example of Ag-Pt plasmonic nanocomposite designed to direct the plasmonic energy from the Ag-core to the thin Pt-shell (Fig. 6a)[52]. Even the localization of charge carriers directly to the catalytic surface does not lead to completion of redox reaction via indirect or direct charge transfer mechanism in the absence of hole scavenger (Fig. 6b, c). However, in the reactions activated by hot electrons, hole scavengers can compensate for the hot hole left behind after the electron injection into the adsorbate from the metal nanoparticle so that the charge separation gets enhanced. Completing the catalytic cycle requires a hole scavenger with a high enough electron-donating capacity to achieve efficient hole extraction (Fig. 6d)[7,54]. The extraction of multiple charge carriers from a plasmonic photocatalyst in the presence of a hole scavenger has also been studied[7]. It has been observed that the

electron-harvesting rate depends upon the photon flux and concentration of the hole scavenger. The kinetics of two competing processes, (i) two-hole scavenging rate and (ii) electron–hole recombination rate, dictates the quantum yield of the two-electron process.

The importance of controlling the transport and lifetime of hot electrons through the Au-polyvinylpyrrolidone (PVP) interface and hot hole scavenging dynamics was established via anisotropic growth of gold nano prisms[55]. Furthermore, the synergistic effect of employing a metal–semiconductor interface (Au/TiO_2) with a hole scavenger (catechol) to carry out a four-hole water oxidation reaction has been presented[56]. In the bare Au/TiO_2 system, both the photogenerated holes and electrons get transferred to TiO_2 (holes get transferred to trap states). As a result, less than 10% of the charge carriers can survive the recombination process resulting in low photocatalytic activity. Hence, to retain hot holes, catechol molecules were adsorbed on the Au surface that could effectively trap plasmon-induced hot holes and assist in driving multi-hole reactions. The role of catechol presents a multi-hole cooperation mechanism where a hole localized on the hole scavenger could drive multi-hole reactions by cooperating with the as-generated hot holes on the plasmonic nanoparticle. Thus, the hole scavenger assists in charge separation and drives oxidation reaction, opening up a new avenue for photochemical processes facilitation.

Moreover, to suppress the recombination rate of plasmon-induced charge carriers and thereby enhance the photocatalytic efficiency of the photocatalysts, various cocatalysts like Pd, Pt, CoO_x can be incorporated that can trap the photogenerated holes or electrons and act as active sites for the oxidation or reduction reactions[57–59].

Among all the systems mentioned above, coupling the plasmonic metal with a semiconductor is a widely studied strategy to achieve effective hot carrier extraction[60]. However, because of their high energy from interband excitations, extraction of hot holes by coupling with a semiconductor offers high merits[61–63]. But because of the challenges posed, only a few works have been reported in this regard[34,35]. In such systems, a promising strategy for reducing the recombination of charge carriers is introducing a passivation layer and forming a metal–insulator–semiconductor (MIS) system that imparts stability when carefully engineered, enhancing the separation of charge carriers[64]. There have been umpteen instances of exploring such insulation interfaces' critical role in improving photocatalytic activity[64–66]. One central virtue in such systems is to find the optimum thickness of the insulator layer so that the charge flux can be optimized, loss via recombination can be suppressed, and the loss of charge carriers through defects or pinholes can be minimized[65,66]. As an instance, Li and coworkers prepared Au/Al_2O_3/TiO_2 photocatalyst and employed it for water oxidation in the presence of $Fe(NO_3)_3$[67]. The Fe^{3+} ions acted as electron acceptors. The photocurrent responses suggested that the Al_2O_3 interface prevented Fe^{2+} ions from getting oxidized by the photogenerated holes, thus promoting water oxidation reaction to an apparent quantum efficiency of 1.3%. Alleviating the need for any external energy inputs, Atwater and coworkers recently fabricated a self-sustaining composite for selective CO_2 reduction to CO via hot hole injection into the p-GaN valence band by introducing an interfacial layer of Al_2O_3 with varying thickness between the Au/p-GaN heterojunction and further depositing Cu nanoparticles on Au surface (Au-Cu/Al_2O_3/p-GaN) (Fig. 6e, f)[60]. The Au/p-GaN has been shown to perform CO_2 reduction; however, the surface defects on the Au/p-GaN interface, which acts as charge recombination sites, reduce the photocatalytic activity. But in Au-Cu/Al_2O_3/p-GaN, the incorporation of Al_2O_3 interfacial layers passivated the surface defects that suppressed
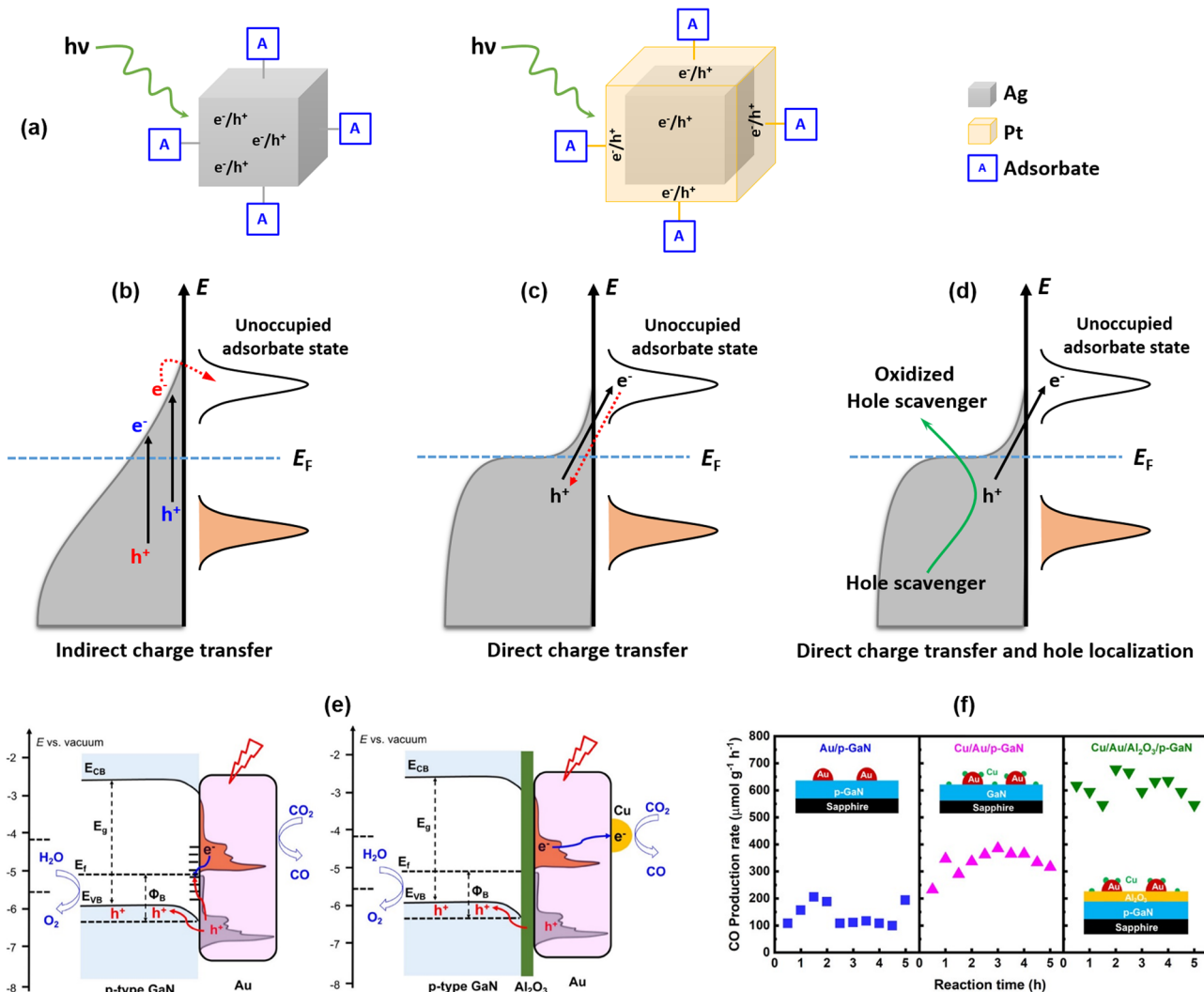
Fig. 6 Importance of charge localization to a catalytic site and hole extraction in photocatalysis. a, Schematic of Ag and Ag-Pt core-shell nanomaterials, the Ag-Pt nanocomposite allows preferential absorption of plasmon energy from the core to the thin Pt-shell, leading to charge generation and extraction in the presence of suitable adsorbate and hole scavenger. **b–d** Illustration of various charge transfer mechanisms. In the absence of hole scavenger both direct and indirect charge transfer mechanism leads to transient charge exchange between nanomaterial and adsorbate; however, the presence of hole scavenger allows permanent ejection of an electron to the adsorbate leading to the catalytic reaction. (**a–d** adapted with permission from ref. [52] copyright © 2019, American Chemical Society). **e** Hot hole injection from Au into the p-GaN valence band and the effect of introducing an interfacial layer of Al_2O_3. The Al_2O_3 interfacial layers passivate the surface defects leading to a longer lifetime of hot carriers. **f** Photocatalytic CO production rate with time highlights 69% enhancement in the Au/Al_2O_3/p-GaN composite rate compared to Au/p-GaN (**e**, **f** reprinted with permission from ref. [60] copyright © 2021, American Chemical Society).

recombination rate between injected holes in p-GaN and electrons in Au and promoted a longer lifetime of hot carriers. At an optimum thickness of Al_2O_3 layers as 1 nm, 69% enhancement in the CO production rate was obtained on Au/Al_2O_3/p-GaN composite compared to Au/p-GaN.

As already mentioned, with the ultrafast dynamics of hot carriers, their timely extraction and storage long enough for any chemical reaction become a difficult task. For this purpose, with an established mechanism of injection of charge carriers into the conduction band or valence band of a semiconductor, various other strategies have also been studied lately[41]. Plasmon-induced metal-to-semiconductor interfacial charge-transfer transition pathway for hot electron transfer has been demonstrated in CdSe-Au nanorod heterostructures (Fig. 7a, b)[41]. In this pathway, the plasmon decay allowed the generation of an electron directly in the semiconductor's conduction band and a hole in the metal owing to strong coupling between the metal and the

semiconductor. In the absence of a hole scavenger, the recombination of electron and hole occurs within 1.45 ps, whereas in the presence of a hole scavenger, CdSe could efficiently reduce methyl viologen. In another recent work, Khurgin et al.[68] explored the mechanism of direct excitation of charge carriers into the adsorbate surface states at a higher rate than the indirect injection of carriers into the adsorbate states (Fig. 7c). These studies have opened new pathways to evade energy losses[54,69,70].

Recently copper chalcogenide nanocrystals have garnered attention for their outstanding hole-based absorption in the near-infrared region[71,72]. A novel multistep plasmon-induced transit charge transfer (PITCT) mechanism was proposed while describing the behavior of hot holes in CdS/CuS heterostructured nanocrystals (HNCs)[50]. The plasmon-induced hole transfer rate was found to be of the order of $10^9 \, s^{-1}$. Although the hole transfer rate was much slower than the hot hole decay rate in CuS, the high quantum efficiency of 19% was obtained, suggesting
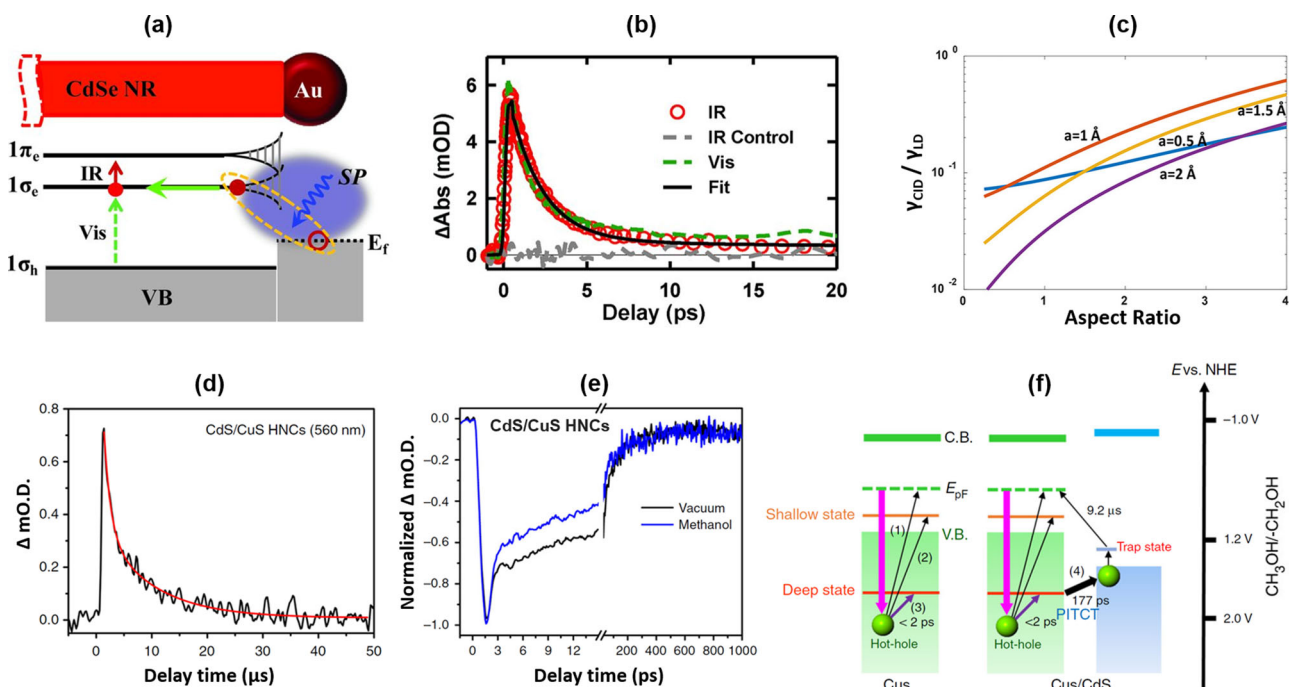
Fig. 7 Novel mechanisms to overcome charge recombination. a Schematic electronic energy diagram for strongly coupled Au-CdSe nanocomposite and direct plasmon-induced metal-to-semiconductor interfacial charge-transfer transition (**a**, **b** from ref. [41] reprinted with permission from AAAS). **b** The intraband absorption feature (red circle) and 1Σ-exciton-bleach (green dashed line) after excitation at 800 nm confirmed the presence of electrons in CdSe. The gray dashed line is a control for the mixture of CdSe NRs and Au nanoparticles. **c** Direct excitation of charge carriers into the adsorbate surface states. The ratio of chemical interface damping rates and Landau damping rates is a function of the aspect ratio of an ellipsoid nanoparticle (reprinted with permission from ref. [68] Copyright © 2021, American Chemical Society). **d–f** highlight a novel multistep PITCT mechanism resulting in long-lived charge separations. **d** Transient absorption for CdS/CuS HNCs tracking holes generated in the CdS phase where it gets trapped, leading to microsecond charge separation. **e** Transient absorption probing LSPR recovery rate: in CdS/CuS HNCs, the improved charge separation allows methanol to scavenge holes efficiently, leading to a substantial increase in LSPR recovery. **f** Schematic of various decay pathways for hot holes generated in CuS NCs and CdS/CuS HNCs (**d–f** reprinted from ref. [50]).

the hole transfer mechanism to be stepwise through carrier trapping states rather than direct injection into the CdS valence band. It was proposed that the hot holes in the deep trap state of CuS were transferred to the CdS valence band that then traversed to the trap state of CdS, leading to microsecond charge separation (Fig. 7d). In the presence of methanol, a slight enhancement in the LSPR recovery rate was observed in CuS nanocrystals. A substantial increase was observed in the case of CdS/CuS HNCs that implied improved charge separation so that methanol could scavenge holes efficiently (Fig. 7e). So, with the help of trap states, the PITCT mechanism allowed the stepwise transfer of hot holes (Fig. 7f) with high quantum efficiency and thus, provided a plausible solution to the prevailing problem of ultrafast relaxation and recombination of hot carriers.

Hot holes in plasmonic catalysis

Polymerization reaction. While extending the applications of plasmonic nanoparticles towards photochemical reactions, the potential of hot holes as oxidants has been realized to perform reactions such as oxygen evolution reaction, polymerization, and oxidation of organic species. In any photochemical reaction, it is essential to quantify the energy of hot carriers at the metal–reactant interface[73]. Although, in principle, the maximum energy of the hot carriers upon their generation is equivalent to the incident photon energy, their effective energy at the metal–molecule interface does not even exceed 50% of the incident energy experimentally because of the apparent energy loss in the carrier transport and extraction[3,74]. An energy screening study with Au nanoparticles for the electro-polymerization

reaction of aniline to conductive polymer polyaniline was performed (Fig. 8a)[12]. The threshold potential for the start of the reaction was obtained as 0.679 V in the dark. However, upon plasmon excitation, polymerization could be achieved at a lower potential of 0.5 V, reducing the threshold potential to be 0.44 V. The plasmon-generated hot holes were the main contributor to such a photocatalytic effect. Notably, under the PICS mechanism, the oxidation potential of plasmonic hot holes has also been realized for oxidative polymerization reactions[75]. Utilizing Au/TiO₂ interface, the oxidative polymerization of pyrrole to conductive polypyrrole has been demonstrated[76]. The feasibility of these reactions while considering the wavelength of excitation, interface band structure, the Fermi level of the metal nanoparticle under illumination, and the energetics of adsorbate molecule relative to the charge carriers strengthen our understanding of plasmon-enhanced catalysis (Fig. 8b)[77].

Water oxidation reaction. By employing plasmonic metal nanostructures as a photoanode material, harvesting energetic holes may impart a solution to clean and sustainable energy. In this regard, Au nanoparticles supported on TiO₂ (Au/TiO₂) is one of the most investigated and efficient systems as photoanode material for water oxidation[78–80]. Formation of a Schottky barrier at Au/TiO₂ interface facilitates electron–hole separation by selectively injecting hot electrons to TiO₂ (H₂ generation site). Hot holes left in Au nanoparticles build the required potential to generate O₂ from water[81,82]. It has been demonstrated that smaller size or having sharp vertices of AuNPs can generate intensified near fields, enabling significant hot holes generation, resulting in improved efficiency of the water oxidation process[83,84]. Besides lifetime and energetics, the spatial
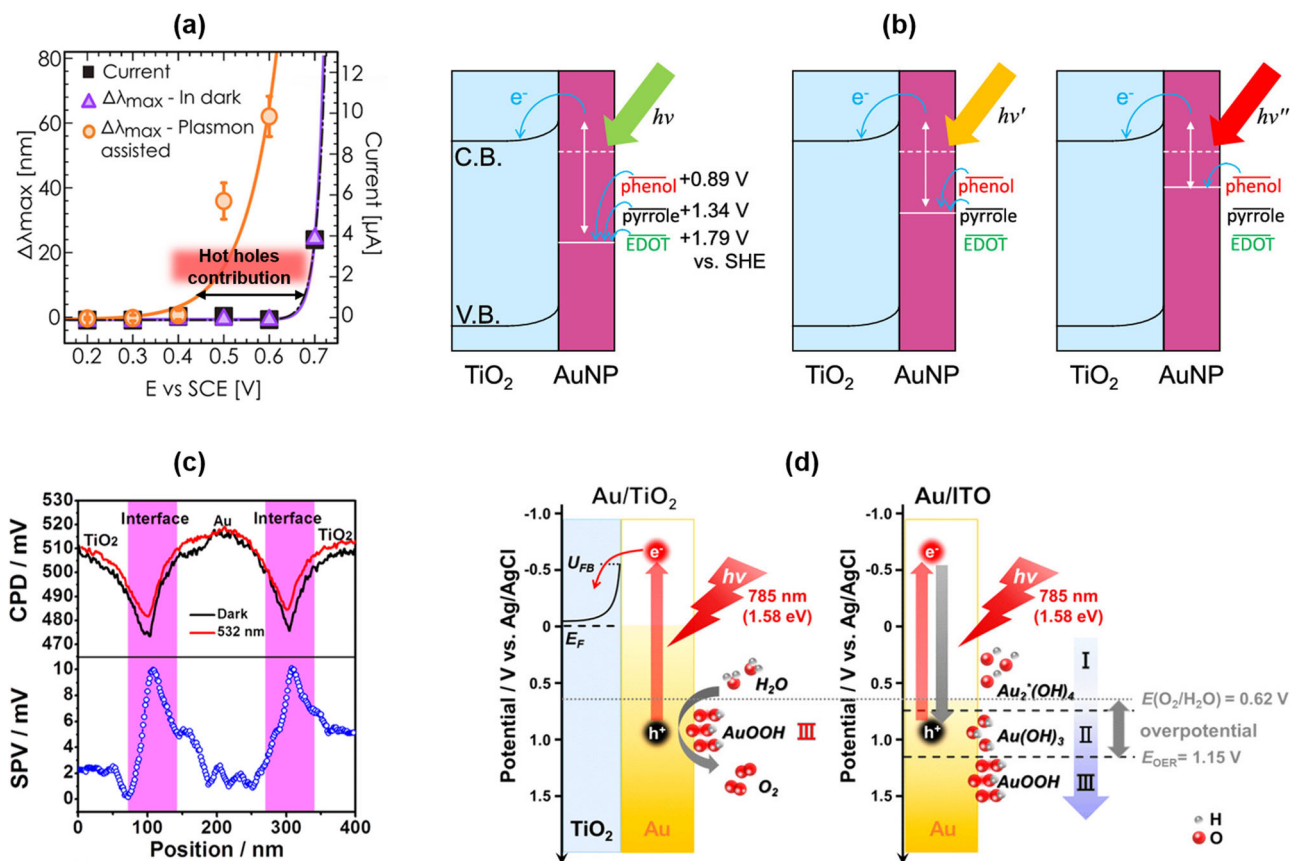
9

Fig. 8 Hot holes-driven polymerization and water oxidation reaction. a Change in the maximum scattering wavelength ($\Delta\lambda_{max}$) as a function of working electrode potential: the obtained threshold for polymerization reaction is 0.68 V in the dark and 0.44 V upon plasmon excitation (reprinted with permission from ref. [12] Copyright © 2019, American Chemical Society). **b** For the Au/TiO$_2$ interface, the excitation with different wavelengths results in hot holes with variable oxidation power that can polymerize monomers/adsorbates depending on their energetics relative to the hole (reprinted with permission from ref. [77] copyright © 2020, American Chemical Society). **c** Contact potential difference (CPD) for the dark state (black line) and state exposed with 532 nm light (red line). The surface photovoltage (SPV) profile across the Au/TiO$_2$ particle indicates plasmonic holes creation near the gold–semiconductor interface (reprinted with permission from ref. [63] copyright © 2017, American Chemical Society). **d** Energy diagram of Au/TiO$_2$ and Au/ITO systems. The oxidation of water proceeds with a single intermediate in the Au/TiO$_2$ system with less overpotential than the Au/ITO system (reprinted with permission from ref. [87] copyright © 2020, American Chemical Society).

distribution of hot holes at the metal–semiconductor interface is impelled to target oxidative reactions with high efficacy and selectivity. Using Kelvin probe force microscopy, Wang et al.[63] probed the separation, transportation, and recombination of plasmon-induced charges within nanometer-scale spatial resolution. They demonstrated that plasmonic holes were mainly concentrated near the gold–semiconductor interface (Fig. 8c). Metal–semiconductor has further been modified with oxygen evolution catalyst, cocatalysts, and hole transporter to perform water oxidation reaction with increased efficacy[56,85,86].

Recently, the plasmonic hot hole-driven water oxidation reaction is being probed under in-situ surface-enhanced Raman spectroscopy to get insights on the reaction intermediates evolving during the reaction. The oxidation at Au/ITO was found to be a multistep process with increased oxidation potential (Au$_2$*(OH)$_4$, Au(OH)$_3$, AuOOH, as reaction intermediates). In contrast, the oxidation process at Au/TiO$_2$ under NIR illumination (1.58 eV) proceeded with a single intermediate (AuOOH) at −0.6 V and pH 7. This shows that water oxidation at Au/TiO$_2$ electrode under NIR light proceeds with less overpotential than Au/ITO, highlighting the occurrence of electron–hole separation via injection of a hot electron to TiO$_2$ and consumption hot holes at Au surface and via water oxidation (Fig. 8d)[87]. Although, Au/TiO$_2$ interface has dominated the field of water oxidation, new

semiconducting material such as BiOCl and MXene (Ti$_3$C$_2$T$_x$) have also been interfaced with plasmonic Ag or Au nanoparticles to demonstrate the synergistic effect of Schottky junction and plasmon-induced hot hole injection, resulting in a significant decrease in the onset overpotential to 0.39 V for the water oxidation reaction[88,89].

Hole-assisted nanoparticle evolution and dissolution. The role of LSPR equivalent to a chemical aid in guiding site-specific controlled growth of nanostructures is widely accepted[90,91]. The site-specific growth of metal nanostructures is a cumulative effect of plasmonic hot charge carriers and facet-specific surfactants/ions present in the growth solution[55,92,93]. Wei and coworkers observed a cooperative effect between the hot holes and the surface adsorbate (iodide ions)[14]. Iodide ions strongly adsorbed on Au seed nanoparticle surface forming Au-iodide, which stabilized the plasmon-generated hot holes and triggered oxidative etching of high index facets of Au (0). In contrast, the low index facets grew, resulting in Au nanostar (Fig. 9a, b). Plasmon-generated hot holes have also been explored to oxidize the metal nanoparticle surface by strategically varying the potential of hot holes. Oxidative dissolution of Au nanorods in an electrochemical process has been investigated. The plasmonic hot holes were taken up by Cl$^-$ ions adsorbed on the Au surface, resulting in
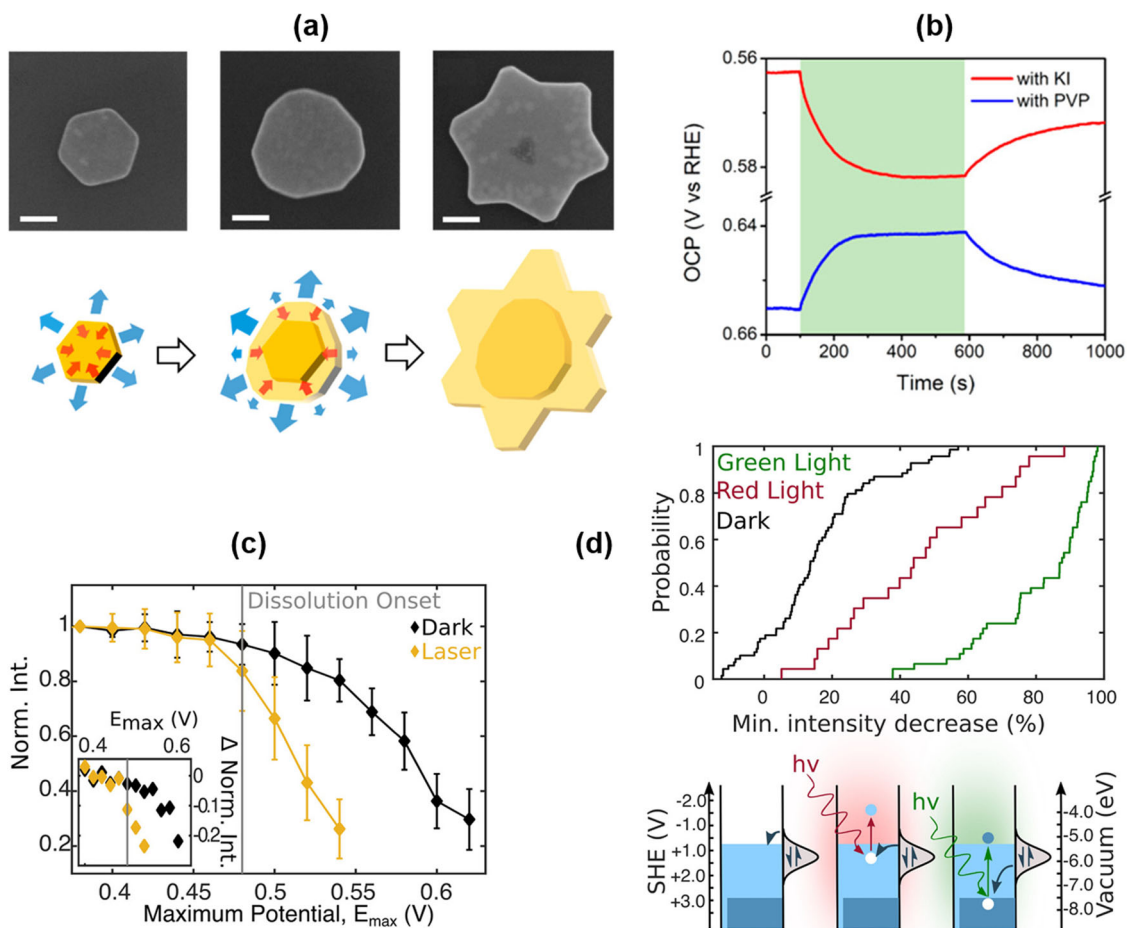
Fig. 9 Plasmon-assisted growth and dissolution of nanoparticles. a Plasmon-driven structure evolution of Au nanoparticle. The hot-electron-driven deposition of Au(0) results in gradual growth (blue arrows), and hot-hole-driven preferential etching results in truncation (blue arrows). **b** Open circuit potential (OCP) measurement of Au nanoparticle in the presence of KI and PVP, respectively (shaded area represents light irradiation). The anodic change in the presence of iodide suggests hot holes trapping by surface Au-iodide species. In contrast, the cathodic change in the presence of PVP represents the trapping of hot electrons by PVP (**a**, **b** reprinted with permission from ref. [14] copyright © 2020, American Chemical Society). **c**, **d** Hot-hole-assisted oxidative electrodissolution of Au nanorod. **c** Dissolution onset potential in the presence and absence of light monitored following the normalized average scattering intensity. **d** Depending upon the excitation wavelength of light, the hot carrier energy distribution changes. The energetic hot holes from the *d*-band (with green light) can cause faster dissolution (resulting in scattering intensity decrease) than the holes near the Fermi level (**c**, **d** reprinted with permission from ref. [31] Copyright © 2019, American Chemical Society).

oxidation of Au (0) to Au (I). The extent of dissolution depends on the potential of holes. It has been demonstrated that the energetic hot holes from the *d*-band of Au drove the reaction more efficiently than the holes near the Fermi level (Fig. 9c, d)[31].

Hole-assisted organic reactions. Recent years have seen a surge in the reports of plasmonic catalysis in organic synthesis or transformations[94,95]. In plasmon-assisted chemical transformations, the plasmonic nanocomposites work as catalysts and provide a platform to follow reaction intermediates due to their excellent SERS properties. The conversion of para-amino thiophenol, PATP to DMAB on Ag nanoparticle has been studied in detail and presented as a model reaction for plasmon driven organic transformation. While probing the reaction mechanism via scavenger-assisted strategy, it has been concluded that the plasmon-generated hot holes are responsible for the oxidative conversion of PATP to DMAB (Fig. 10a)[96]. Recently, we demonstrated Au NPs catalyzed oxidative coupling of benzylamine to N-benzylidenebenzylamine with 64% conversion efficiency. The activation of both the reactants amine and O_2 via capturing hot holes and electrons, respectively, and catalyzing C=N bond formation has solely been governed by Au NPs

(Fig. 10b)[13]. The wavelength-dependent excitation of AuNPs allows the variation of potential energy accessible to charge carriers. And the maximum conversion efficiency was obtained for interband excitation with highly energetic *d*-band holes.

Oxidative transformations of benzyl alcohol to benzaldehyde are another reactions that have been performed, availing the oxidizing ability of plasmonic hot holes. Out of the possible combinations, plasmonic photocatalyst, which strongly interacts with molecular O_2 and generates mild oxidative holes, may impart high selectivity to alcohol oxidation[97,98]. Careful design of BiOCl possessing high oxygen vacancies was exploited as support for Au NPs to provide charge separation and activation of O_2. Au-BiOCl excitation results in the synergistic effect of plasmonic hot electrons and holes where hot electrons trapped in oxygen vacancies produce surface-bound $O_2^{\bullet-}$ and the hot holes on Au NPs abstract α-H of benzyl alcohol to form a carbon-centered radical which combines with adjacent $O_2^{\bullet-}$ radical which ultimately leads to the formation of benzaldehyde (Fig. 10c)[99].

Outlook. With the realization of plasmon-generated hot-electrons and hot-holes, many hybrid plasmonic nanocomposites
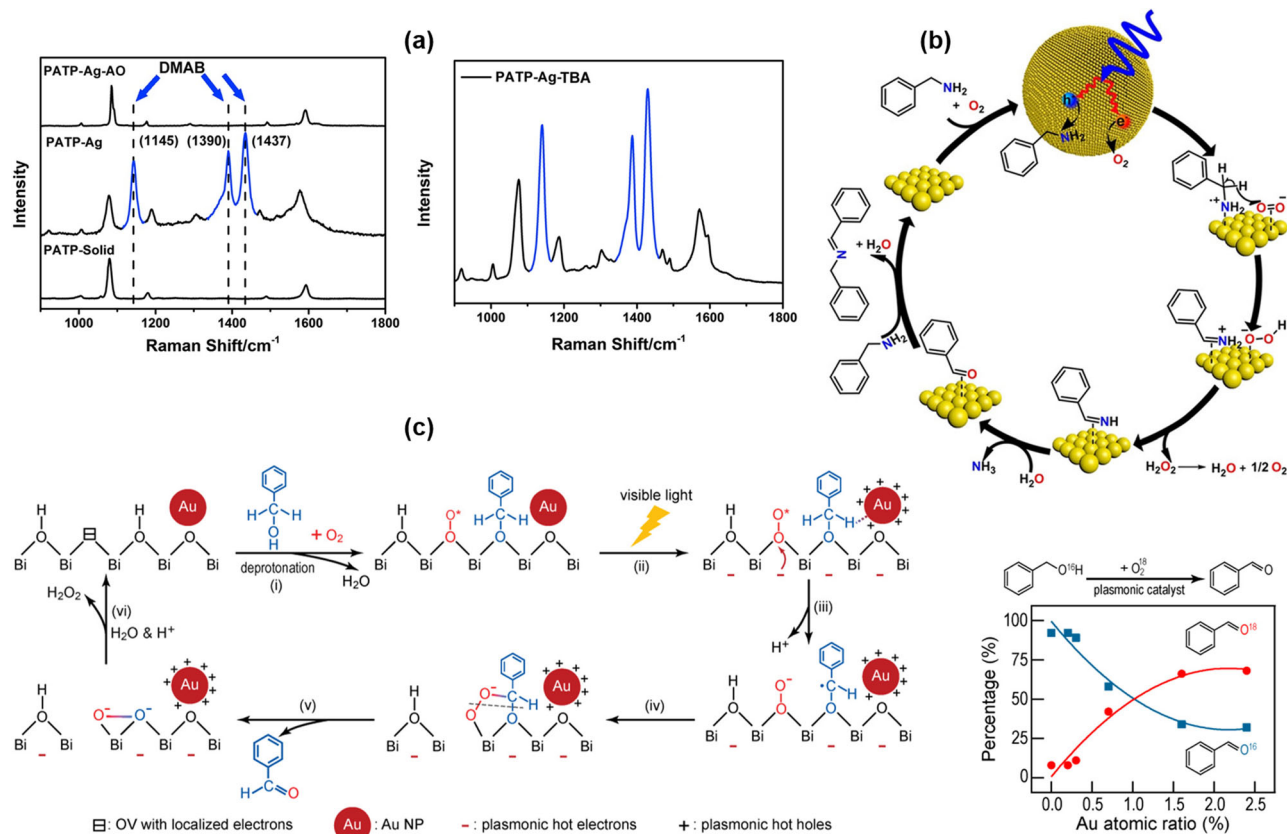
Fig. 10 Hot-holes driven organic reactions. a SERS demonstrating the oxidative conversion of PATP to DMAB on Ag nanoparticle. In the presence of ammonium oxalate (AO), a hole scavenger, the conversion does not occur, whereas in the presence of t-butanol (TBA), a hydroxyl radical scavenger, the reaction occurs. These observations suggest that holes drive the reaction (reprinted from ref. [96]). **b** Plausible mechanism of plasmon-enhanced oxidative coupling reaction of benzylamine to N-benzylidenebenzylamine (imine), where the activation of both the reactants amine and O_2 occurs via capturing hot holes and electrons (reprinted with permission from ref. [13]). **c** Plasmon-driven benzyl alcohol to benzaldehyde conversion on Au-BiOCl. Upon excitation, the oxygen vacancy on BiOCl traps the hot electron and synergistically the hot holes on Au NPs abstract α-H of benzyl alcohol which ultimately leads to the formation of benzaldehyde. The yield of ^{18}O leveled benzaldehyde increases with the increase in the loading of Au in Au-BiOCl (reprinted with permission from ref. [99] copyright © 2017, American Chemical Society).

have been designed to extract these charge carriers to drive surface chemistry, including polymerization, water oxidation, nanoparticle growth and dissolution, and various organic reaction. However, the true promise of plasmonic catalysis lies in the ability to localize the plasmon energy at the catalytic site to effectively excite a specific electronic transition at the nanocomposite/reactant interface leading to much-desired product selectivity. The localization of charge carriers at the catalytic site is critical for hole-assisted plasmonic catalysis because of their ultrashort lifetime, faster relaxation dynamics, and shorter mean free path. Metal–metal, metal–semiconductor, metal-molecule, and other nanocomposite systems have been engineered to control the initial generation of charge carriers directly at the interface to overcome the limitations mentioned above. In this regard, Linic and coworkers have provided the following guiding principles which needs to be considered while designing the nanocomposites: (i) using small plasmonic material so that the surface-collision assisted transition (Kreibig decay) dominates, (ii) designing a plasmonic structure which enables high field enhancement and allows subdiffraction-limit field localization at the surface, (iii) creating the interface with other nonplasmonic metal/semiconductor/molecule with the high imaginary part of the dielectric function and tailored band structure to direct the energy towards the catalytic site preferentially[19,54,100–102].

Theoretical and experimental evidence have depicted that the hot charge carriers' internal energy, momentum distribution, and

energy-dependent mean free path control the charge separation efficacy to drive any chemical reaction. Here one also needs to understand the tradeoff between the generation of hot carriers and their extraction across various interfaces. The interband excitations in plasmonic nanomaterials generate a distribution of electrons localized closer to the Fermi level resulting in lower IQE for hot electron collection despite a long mean free path. While the same interband excitation generates a significant distribution of high-energy d-band holes, which can be extracted, resulting in higher IQE for hot hole collection despite a short mean free path[37]. So, for optimal extraction of hot carriers, along with engineering the interfacial properties, careful consideration needs to be given to the operational regime for the device as well. Few seminal works have demonstrated a long lifetime of d-band holes near the band edge in Cu nanostructures that can exceed the lifetime of sp-band electrons[103,104]. In our view, despite the existing obscurity in the extraction of hot holes, Au and Cu nanostructures hold great promise in collecting and injecting hot d-holes across various nano-heterointerfaces with tailored energetics.

Although these guidelines help design plasmonic nanocomposites, performing selective chemistry depends not only on the nanocomposite design but also on the energetics of reactants–nanocomposite interface, coupling strength of the specific electronic state of the reactant with the nanocomposite. So, to move this field forward, we need a better understanding of

electronic excitations at the interface of catalyst and reactant and atomistic control of energy deposition to a specific electronic state of the reactant. Mainly to realize the potential of highly energetic d-band holes, we must understand the factors governing the dynamics and propagation of charge carriers through the entire nano-heterointerface.

We believe that the single-molecule analyses on both dynamics and energetics of charge transfer across various interfaces will be imperative in elucidating hot-carrier reactivity and charge-transport processes[103,105,106]. A dark-field microscopy correlated with photoelectrochemistry has been employed to track a hot-hole-driven reaction on a single Au nanoparticle. Exploring the energy and spatial distribution of hot carriers at the single-molecule level helps dissect the complex charge transport dynamics across interfaces, which offers nanoscopic insights to design and enhance the performance of photocatalytic systems.

Overall we believe that in addition to the quantum chemical calculations, the use of in situ single-molecule correlated techniques to probe the feasibility of the catalytic reaction on nanocomposite surface by tuning (i) the potential of charge carriers via intraband and interband excitation, (ii) interface structure, (iii) Fermi level of the metal nanoparticle under illumination, and (iv) the energetics of reactant–catalyst interface will be critical for better extraction of charge carriers and to design plasmonic nanocomposites to drive selective chemical reactions.

The development of nano-heterointerfaces capable of confining hot charge carriers at catalytic sites can be a breakthrough for the industrially relevant water oxidation reaction. Plasmonic hot holes generated at Au/TiO$_2$ interface have been shown to generate significant anodic potential to overcome the energy barrier of water oxidation[107]. Additionally, the active interfacial sites support the adsorption and activation of water molecules via generating highly reactive species (e.g., Au–*OH), which sufficiently lowers the overpotential for the water oxidation reaction[87]. Importantly, the choice of interface significantly affects the hole injection process (ultimately the charge separation ability) and changes the reaction efficacy. In essence, the plasmonic nano-heterointerface demands significant attention as it can serve as a powerful platform to target selective chemical reactions of industrial relevance.

References

1. Watanabe, K., Menzel, D., Nilius, N. & Freund, H.-J. Photochemistry on metal nanoparticles. *Chem. Rev.* **106**, 4301–4320 (2006).
2. Khurgin, J. B. Hot carriers generated by plasmons: where are they generated and where do they go from there? *Faraday Discuss* **214**, 35–58 (2019).
3. Brown, A. M., Sundararaman, R., Narang, P., Goddard, W. A. & Atwater, H. A. Nonradiative Plasmon decay and hot carrier dynamics: effects of phonons, surfaces, and geometry. *ACS Nano* **10**, 957–966 (2016). *First principle calculations underlying the surface plasmon decay mechanism and ab-initio predictions for energy distribution of generated hot charge carriers in plasmonic metals.*
4. Narang, P., Sundararaman, R. & Atwater, H. A. Plasmonic hot carrier dynamics in solid-state and chemical systems for energy conversion. *Nanophotonics* **5**, 96–111 (2016).
5. Boudart, M., Davis, B. H. & Heinemann, H. Introduction. in *Handbook of Heterogeneous Catalysis* (John Wiley & Sons, Ltd, 1997).
6. Bonn, M. et al. Phonon- versus electron-mediated desorption and oxidation of CO on Ru(0001). *Science* **285**, 1042–1045 (1999). *An illustration of contrasting reaction pathways on a bulk metal surface when initiated by laser-induced hot substrate electrons in comparison to thermal activation.*
7. Kim, Y., Smith, J. G. & Jain, P. K. Harvesting multiple electron–hole pairs generated through plasmonic excitation of Au nanoparticles. *Nat. Chem.* **10**, 763–769 (2018).
8. Zhang, Y. et al. Surface-plasmon-driven hot electron photochemistry. *Chem. Rev.* **118**, 2927–2954 (2018). *A detailed review emphasizing the role of LPSR decay-generated hot electrons in driving chemical reactions underlying the opportunities and challenges present in the field.*
9. Hartland, G. V. Optical studies of dynamics in noble metal nanostructures. *Chem. Rev.* **111**, 3858–3887 (2011).
10. Khurgin, J. B. Fundamental limits of hot carrier injection from metal in nanoplasmonics. *Nanophotonics* **9**, 453–471 (2020).
11. Graf, M., Vonbun-Feldbauer, G. B. & Koper, M. T. M. Direct and broadband plasmonic charge transfer to enhance water oxidation on a gold electrode. *ACS Nano* **15**, 3188–3200 (2021).
12. Pensa, E. et al. Spectral screening of the energy of hot holes over a particle plasmon resonance. *Nano Lett.* **19**, 1867–1874 (2019).
13. Swaminathan, S., Rao, V. G., Bera, J. K. & Chandra, M. The pivotal role of hot carriers in plasmonic catalysis of C−N bond forming reaction of amines. *Angew. Chem. Int. Ed.* **60**, 12532–12538 (2021). *Demonstration of the role of plasmonic hot charge carriers and excitation-dependent tuning of their potential energy for oxidative C-N bond formation.*
14. Guo, W. et al. Cooperation of hot holes and surface adsorbates in plasmon-driven anisotropic growth of gold nanostars. *J. Am. Chem. Soc.* **142**, 10921–10925 (2020).
15. Halas, N. J., Lal, S., Chang, W.-S., Link, S. & Nordlander, P. Plasmons in strongly coupled metallic nanostructures. *Chem. Rev.* **111**, 3913–3961 (2011).
16. Hao, E. & Schatz, G. C. Electromagnetic fields around silver nanoparticles and dimers. *J. Chem. Phys.* **120**, 357–366 (2004).
17. Linic, S., Christopher, P. & Ingram, D. B. Plasmonic-metal nanostructures for efficient conversion of solar to chemical energy. *Nat. Mater.* **10**, 911–921 (2011).
18. Khurgin, J. B. How to deal with the loss in plasmonics and metamaterials. *Nat. Nanotechnol.* **10**, 2–6 (2015).
19. Linic, S., Chavez, S. & Elias, R. Flow and extraction of energy and charge carriers in hybrid plasmonic nanostructures. *Nat. Mater.* **20**, 916–924 (2021).
20. Abelès, F. *Optical Properties of Solids* (ed. Abeles, F.) (American Elsevier, 1972).
21. Kreibig, U. & Vollmer, M. *Optical Properties of Metal Clusters.* (Springer-Verlag, 1995).
22. Link, S. & El-Sayed, M. A. Spectral properties and relaxation dynamics of surface plasmon electronic oscillations in gold and silver nanodots and nanorods. *J. Phys. Chem. B* **103**, 8410–8426 (1999).
23. Brongersma, M. L., Halas, N. J. & Nordlander, P. Plasmon-induced hot carrier science and technology. *Nat. Nanotechnol.* **10**, 25–34 (2015).
24. Boerigter, C., Aslam, U. & Linic, S. Mechanism of charge transfer from plasmonic nanostructures to chemically attached materials. *ACS Nano* **10**, 6108–6115 (2016). *Development of mechanistic understanding of excitation and flow of charge carriers across a plasmonic metal-molecule interface.*
25. Sundararaman, R., Narang, P., Jermyn, A. S., Goddard III, W. A. & Atwater, H. A. Theoretical predictions for hot-carrier generation from surface plasmon decay. *Nat. Commun.* **5**, 5788 (2014).
26. Bernardi, M., Mustafa, J., Neaton, J. B. & Louie, S. G. Theory and computation of hot carriers generated by surface plasmon polaritons in noble metals. *Nat. Commun.* **6**, 7044 (2015).
27. Jacoboni, C. *Theory of Electron Transport in Semiconductors: A Pathway from Elementary Physics to Nonequilibrium Green Functions* (Springer-Verlag, 2010).
28. Blanco-Rey, M., Alducin, M., Juaristi, J. I. & de Andres, P. L. Diffusion of hydrogen in Pd assisted by inelastic ballistic hot electrons. *Phys. Rev. Lett.* **108**, 115902 (2012).
29. Liu, G., Zhen, C., Kang, Y., Wang, L. & Cheng, H.-M. Unique physicochemical properties of two-dimensional light absorbers facilitating photocatalysis. *Chem. Soc. Rev.* **47**, 6410–6444 (2018).
30. Heilpern, T. et al. Determination of hot carrier energy distributions from inversion of ultrafast pump-probe reflectivity measurements. *Nat. Commun.* **9**, 1853 (2018).
31. Al-Zubeidi, A. et al. Hot holes assist plasmonic nanoelectrode dissolution. *Nano Lett.* **19**, 1301–1306 (2019).
32. Yu, Y., Wijesekara, K. D., Xi, X. & Willets, K. A. Quantifying wavelength-dependent plasmonic hot carrier energy distributions at metal/semiconductor interfaces. *ACS Nano* **13**, 3629–3637 (2019).
33. Reddy, H. et al. Determining plasmonic hot-carrier energy distributions via single-molecule transport measurements. *Science* **369**, 423–426 (2020).
34. DuChene, J. S., Tagliabue, G., Welch, A. J., Cheng, W.-H. & Atwater, H. A. Hot hole collection and photoelectrochemical CO$_2$ reduction with plasmonic Au/p-GaN photocathodes. *Nano Lett.* **18**, 2545–2550 (2018).

35. DuChene, J. S. et al. Optical excitation of a nanoparticle Cu/p-NiO photocathode improves reaction selectivity for CO_2 reduction in aqueous electrolytes. *Nano Lett.* **20**, 2348–2358 (2020).

36. Tagliabue, G. et al. Ultrafast hot-hole injection modifies hot-electron dynamics in Au/p-GaN heterostructures. *Nat. Mater.* **19**, 1312–1318 (2020).

37. Tagliabue, G., DuChene, J. S., Habib, A., Sundararaman, R. & Atwater, H. A. Hot-hole versus hot-electron transport at Cu/GaN heterojunction interfaces. *ACS Nano* **14**, 5788–5797 (2020). **An important comparative study on extraction of hot holes and hot electrons at metal/semiconductor interface highlighting the role of carrier energy and their mean free path.**

38. Cortés, E. et al. Challenges in plasmonic catalysis. *ACS Nano* **14**, 16202–16219 (2020).

39. Tian, Y. & Tatsuma, T. Mechanisms and applications of plasmon-induced charge separation at TiO_2 films loaded with gold nanoparticles. *J. Am. Chem. Soc.* **127**, 7632–7637 (2005).

40. Takahashi, Y. & Tatsuma, T. Solid state photovoltaic cells based on localized surface plasmon-induced charge separation. *Appl. Phys. Lett.* **99**, 182110 (2011).

41. Wu, K., Chen, J., McBride, J. R. & Lian, T. Efficient hot-electron transfer by a plasmon-induced interfacial charge-transfer transition. *Science* **349**, 632–635 (2015). **Experimental evidence of direct electron transfer *via* LSPR decay at strongly coupled metal/semiconductor interface.**

42. Govorov, A. O., Zhang, H. & Gun'ko, Y. K. Theory of photoinjection of hot plasmonic carriers from metal nanostructures into semiconductors and surface molecules. *J. Phys. Chem. C* **117**, 16616–16631 (2013).

43. Tatsuma, T., Nishi, H. & Ishida, T. Plasmon-induced charge separation: chemistry and wide applications. *Chem. Sci.* **8**, 3325–3337 (2017).

44. Kazuma, E., Sakai, N. & Tatsuma, T. Nanoimaging of localized plasmon-induced charge separation. *Chem. Commun.* **47**, 5777–5779 (2011).

45. Tatsuma, T. & Nishi, H. Plasmonic hole ejection involved in plasmon-induced charge separation. *Nanoscale Horiz.* **5**, 597–606 (2020).

46. Ishida, T., Toe, S. & Tatsuma, T. Stepwise injection of energetic electrons and holes in plasmon-induced charge separation. *J. Phys. Chem. C* **123**, 30562–30570 (2019).

47. Barman, T., Hussain, A. A., Sharma, B. & Pal, A. R. Plasmonic hot hole generation by interband transition in gold-polyaniline. *Sci. Rep.* **5**, 18276 (2015).

48. Reineck, P. et al. A solid-state plasmonic solar cell via metal nanoparticle self-assembly. *Adv. Mater.* **24**, 4750–4755 (2012).

49. Lee, S. H., Nishi, H. & Tatsuma, T. Plasmonic behaviour and plasmon-induced charge separation of nanostructured MoO_{3-x} under near infrared irradiation. *Nanoscale* **10**, 2841–2847 (2018).

50. Lian, Z. et al. Near infrared light induced plasmonic hot hole transfer at a nano-heterointerface. *Nat. Commun.* **9**, 2314 (2018). **An experimental report on high quantum yields and long-lived charge separation via plasmon-induced transit carrier transfer mechanism in CdS/CuS heterostructures.**

51. Lee, D. & Yoon, S. Plasmonic switching: hole transfer opens an electron-transfer channel in plasmon-driven reactions. *J. Phys. Chem. C* **124**, 15879–15885 (2020).

52. Xie, W., Herrmann, C., Kömpe, K., Haase, M. & Schlücker, S. Synthesis of bifunctional Au/Pt/Au core/shell nanoraspberries for in situ SERS monitoring of platinum-catalyzed reactions. *J. Am. Chem. Soc.* **133**, 19302–19305 (2011).

53. Xie, W. & Schlücker, S. Hot electron-induced reduction of small molecules on photorecycling metal surfaces. *Nat. Commun.* **6**, 7570 (2015).

54. Rao, V. G., Aslam, U. & Linic, S. Chemical requirement for extracting energetic charge carriers from plasmonic metal nanoparticles to perform electron-transfer reactions. *J. Am. Chem. Soc.* **141**, 643–647 (2019).

55. Zhai, Y. et al. Polyvinylpyrrolidone-induced anisotropic growth of gold nanoprisms in plasmon-driven synthesis. *Nat. Mater.* **15**, 889–895 (2016).

56. Zhang, Y. et al. Modulating multi-hole reaction pathways for photoelectrochemical water oxidation on gold nanocatalysts. *Energy Environ. Sci.* **13**, 1501–1508 (2020).

57. Jiang, W. et al. Integration of multiple plasmonic and cocatalyst nanostructures on TiO_2 nanosheets for visible-near-infrared photocatalytic hydrogen evolution. *Small* **12**, 1640–1648 (2016).

58. Okazaki, M. et al. Site-selective deposition of a cobalt cocatalyst onto a plasmonic Au/TiO_2 photoanode for improved water oxidation. *ACS Appl. Energy Mater.* **3**, 5142–5146 (2020).

59. Kao, K.-C., Kuroiwa, Y., Nishi, H. & Tatsuma, T. Hydrogen evolution from water based on plasmon-induced charge separation at a TiO_2/Au/NiO/Pt system. *Phys. Chem. Chem. Phys.* **19**, 31429–31435 (2017).

60. Li, R. et al. Unassisted highly selective gas-phase CO_2 reduction with a plasmonic Au/p-GaN photocatalyst using H_2O as an electron donor. *ACS Energy Lett.* **6**, 1849–1856 (2021).

61. Tanaka, A., Teramura, K., Hosokawa, S., Kominami, H. & Tanaka, T. Visible light-induced water splitting in an aqueous suspension of a plasmonic Au/TiO_2 photocatalyst with metal cocatalysts. *Chem. Sci.* **8**, 2574–2580 (2017).

62. Zhan, C. et al. Interfacial construction of plasmonic nanostructures for the utilization of the plasmon-excited electrons and holes. *J. Am. Chem. Soc.* **141**, 8053–8057 (2019).

63. Wang, S. et al. Positioning the water oxidation reaction sites in plasmonic photocatalysts. *J. Am. Chem. Soc.* **139**, 11771–11778 (2017).

64. Quinn, J., Hemmerling, J. & Linic, S. Maximizing solar water splitting performance by nanoscopic control of the charge carrier fluxes across semiconductor–electrocatalyst junctions. *ACS Catal.* **8**, 8545–8552 (2018).

65. Hemmerling, J. R., Mathur, A. & Linic, S. Design principles for efficient and stable water splitting photoelectrocatalysts. *Acc. Chem. Res.* **54**, 1992–2002 (2021).

66. Kontoleta, E. et al. Using hot electrons and hot holes for simultaneous cocatalyst deposition on plasmonic nanostructures. *ACS Appl. Mater. Interfaces* **12**, 35986–35994 (2020).

67. Zeng, B. et al. Interfacial modulation with aluminum oxide for efficient plasmon-induced water oxidation. *Adv. Funct. Mater.* **31**, 2005688 (2021).

68. Khurgin, J. B., Petrov, A., Eich, M. & Uskov, A. V. Direct plasmonic excitation of the hybridized surface states in metal nanoparticles. *ACS Photonics* **8**, 2041–2049 (2021).

69. Boerigter, C., Campana, R., Morabito, M. & Linic, S. Evidence and implications of direct charge excitation as the dominant mechanism in plasmon-mediated photocatalysis. *Nat. Commun.* **7**, 10545 (2016).

70. Kale, M. J., Avanesian, T., Xin, H., Yan, J. & Christopher, P. Controlling catalytic selectivity on metal nanoparticles by direct photoexcitation of adsorbate–metal bonds. *Nano Lett.* **14**, 5405–5412 (2014).

71. Xie, Y. et al. Metallic-like stoichiometric copper sulfide nanocrystals: phase- and shape-selective synthesis, near-infrared surface plasmon resonance properties, and their modeling. *ACS Nano* **7**, 7352–7369 (2013).

72. Luther, J. M., Jain, P. K., Ewers, T. & Alivisatos, A. P. Localized surface plasmon resonances arising from free carriers in doped quantum dots. *Nat. Mater.* **10**, 361–366 (2011).

73. Cortés, E. Efficiency and bond selectivity in plasmon-induced photochemistry. *Adv. Opt. Mater.* **5**, 1700191 (2017).

74. Kim, Y., Dumett Torres, D. & Jain, P. K. Activation energies of plasmonic catalysts. *Nano Lett.* **16**, 3399–3407 (2016).

75. Minamimoto, H. et al. Visualization of active sites for plasmon-induced electron transfer reactions using photoelectrochemical polymerization of pyrrole. *J. Phys. Chem. C* **120**, 16051–16058 (2016).

76. Takahashi, Y., Furukawa, Y., Ishida, T. & Yamada, S. Site-selective nanoscale-polymerization of pyrrole on gold nanoparticles via plasmon induced charge separation. *Nanoscale* **8**, 8520–8524 (2016).

77. Takahashi, Y., Sota, Y., Ishida, T., Furukawa, Y. & Yamada, S. Oxidative reaction energy in photopolymerization inspired by plasmon-induced charge separation. *J. Phys. Chem. C* **124**, 4202–4205 (2020).

78. Warren, S. C. & Thimsen, E. Plasmonic solar water splitting. *Energy Environ. Sci.* **5**, 5133–5146 (2012).

79. Shi, X., Ueno, K., Takabayashi, N. & Misawa, H. Plasmon-enhanced photocurrent generation and water oxidation with a gold nanoisland-loaded titanium dioxide photoelectrode. *J. Phys. Chem. C* **117**, 2494–2499 (2013).

80. Pu, Y.-C. et al. Au nanostructure-decorated TiO_2 nanowires exhibiting photoactivity across entire UV-visible region for photoelectrochemical water splitting. *Nano Lett.* **13**, 3817–3823 (2013).

81. Gomes Silva, C., Juárez, R., Marino, T., Molinari, R. & García, H. Influence of excitation wavelength (UV or visible light) on the photocatalytic activity of titania containing gold nanoparticles for the generation of hydrogen or oxygen from water. *J. Am. Chem. Soc.* **133**, 595–602 (2011).

82. Lee, H., Song, K., Lee, M. & Park, J. Y. In situ visualization of localized surface plasmon resonance-driven hot hole flux. *Adv. Sci.* **7**, 2001148 (2020).

83. Moon, C. W. et al. Plasmonic octahedral gold nanoparticles of maximized near electromagnetic fields for enhancing catalytic hole transfer in solar water splitting. *Part. Part. Syst. Charact.* **34**, 1600340 (2017).

84. Teranishi, M., Wada, M., Naya, S. & Tada, H. Size-dependence of the activity of gold nanoparticle-loaded titanium(IV) oxide plasmonic photocatalyst for water oxidation. *ChemPhysChem* **17**, 2813–2817 (2016).

85. Lee, J., Mubeen, S., Ji, X., Stucky, G. D. & Moskovits, M. Plasmonic photoanodes for solar water splitting with visible light. *Nano Lett.* **12**, 5014–5019 (2012).

86. Ha, H. D. et al. Precise colloidal plasmonic photocatalysts constructed by multistep photodepositions. *Nano Lett.* **20**, 8661–8667 (2020).

87. Suzuki, K., Li, X., Wang, Y., Nagasawa, F. & Murakoshi, K. Active intermediates in plasmon-induced water oxidation at Au nanodimer structures on a single crystal of TiO_2. *ACS Energy Lett.* **5**, 1252–1259 (2020).

88. Bai, S. et al. Toward enhanced photocatalytic oxygen evolution: synergetic utilization of plasmonic effect and Schottky junction via interfacing facet selection. *Adv. Mater.* **27**, 3444–3452 (2015).

89. Wang, J. et al. Plasmonic Au nanoparticle@$Ti_3C_2T_x$ heterostructures for improved oxygen evolution performance. *Inorg. Chem.* **60**, 5890–5897 (2021).

90. Jin, R. Photoinduced conversion of silver nanospheres to nanoprisms. *Science* **294**, 1901–1903 (2001).

91. Xue, C., Métraux, G. S., Millstone, J. E. & Mirkin, C. A. Mechanistic study of photomediated triangular silver nanoprism growth. *J. Am. Chem. Soc.* **130**, 8337–8344 (2008).

92. Maillard, M., Huang, P. & Brus, L. Silver nanodisk growth by surface plasmon enhanced photoreduction of adsorbed [Ag $^+$]. *Nano Lett.* **3**, 1611–1615 (2003).

93. Langille, M. R., Personick, M. L. & Mirkin, C. A. Plasmon-mediated syntheses of metallic nanostructures. *Angew. Chem. Int. Ed.* **52**, 13910–13940 (2013).

94. Wang, C. & Astruc, D. Nanogold plasmonic photocatalysis for organic synthesis and clean energy conversion. *Chem. Soc. Rev.* **43**, 7188–7216 (2014).

95. Hao, C.-H. et al. Visible-light-driven selective photocatalytic hydrogenation of cinnamaldehyde over Au/SiC catalysts. *J. Am. Chem. Soc.* **138**, 9361–9364 (2016).

96. Yan, X., Wang, L., Tan, X., Tian, B. & Zhang, J. Surface-enhanced raman spectroscopy assisted by radical capturer for tracking of plasmon-driven redox reaction. *Sci. Rep.* **6**, 30193 (2016).

97. Zhang, M., Chen, C., Ma, W. & Zhao, J. Visible-light-induced aerobic oxidation of alcohols in a coupled photocatalytic system of dye-sensitized TiO$_2$ and TEMPO. *Angew. Chem. Int. Ed.* **47**, 9730–9733 (2008).

98. Choi, W. Pure and modified TiO$_2$ photocatalysts and their environmental applications. *Catal. Surv. Asia* **10**, 16–28 (2006).

99. Li, H. et al. New reaction pathway induced by plasmon for selective benzyl alcohol oxidation on BiOCl possessing oxygen vacancies. *J. Am. Chem. Soc.* **139**, 3513–3521 (2017).

100. Chavez, S., Aslam, U. & Linic, S. Design principles for directing energy and energetic charge flow in multicomponent plasmonic nanostructures. *ACS Energy Lett.* **3**, 1590–1596 (2018).

101. Chavez, S., Govind Rao, V. & Linic, S. Unearthing the factors governing site specific rates of electronic excitations in multicomponent plasmonic systems and catalysts. *Faraday Discuss* **214**, 441–453 (2019).

102. Aslam, U., Rao, V. G., Chavez, S. & Linic, S. Catalytic conversion of solar to chemical energy on plasmonic metal nanostructures. *Nat. Catal.* **1**, 656–665 (2018). *A systematic overview of recent developments and scope in plasmonic catalysis emphasizing guiding principles for designing new hybrid nanostructures to improve extraction of hot charge carriers and target selective chemical transformations.*

103. Cai, Y.-Y. et al. Single-particle emission spectroscopy resolves d-hole relaxation in copper nanocubes. *ACS Energy Lett.* **4**, 2458–2465 (2019).

104. Petek, H., Nagano, H. & Ogawa, S. Hole decoherence of *d* bands in copper. *Phys. Rev. Lett.* **83**, 832–835 (1999).

105. Govind Rao, V. & Lu, H. P. Inhomogeneous and complex interfacial electron-transfer dynamics: a single-molecule perspective. *ACS Energy Lett.* **1**, 773–791 (2016).

106. Simoncelli, S. et al. Monitoring plasmonic hot-carrier chemical reactions at the single particle level. *Faraday Discuss* **214**, 73–87 (2019).

107. Hung, S.-F. et al. Iridium oxide-assisted plasmon-induced hot carriers: improvement on kinetics and thermodynamics of hot carriers. *Adv. Energy Mater.* **6**, 1501339 (2016).

Acknowledgements

Author contributions

V.G.R. proposed and supervised the idea. V.G.R. and M.A. conceptualized the proposal. M.A. and D.M. wrote the first draft of the manuscript and V.G.R. revised the manuscript. All authors provided critical feedback at the stage of revisions.

Competing interests

The authors declare no competing interests.

Additional information

Supplementary information The online version contains supplementary material available at https://doi.org/10.1038/s43246-021-00220-4.

Correspondence and requests for materials should be addressed to Vishal Govind Rao.

Peer review information: *Communications Materials* thanks Emiliano Cortés and the other, anonymous, reviewer for their contribution to the peer review of this work. Primary Handling Editor: John Plummer. Peer reviewer reports are available.

Reprints and permission information is available at http://www.nature.com/reprints

Publisher's note Springer Nature remains neutral with regard to jurisdictional claims in published maps and institutional affiliations.